IEEE Access
Multidisciplinary | Rapid Review | Open Access Journal

Received 9 February 2024, accepted 26 February 2024, date of publication 29 February 2024, date of current version 6 March 2024.

Digital Object Identifier 10.1109/ACCESS.2024.3371571

RESEARCH ARTICLE

Compact Circular-Shaped MIMO Antenna Covers UWB Bandwidth With Four Frequently-Used Band-Notched Characteristics for Multi-Scenario Applications

LIANGLIANG ZHAO[1], YONGMAO WANG[1], CHENLU LIU[1], DENGYANG SONG[1], CHUFENG HU[2], CHUWEI LI[3], HUILING ZHAO[1], AND ZEFANG WANG[1]

[1]School of Electronics and Information, Northwestern Polytechnical University, Xi'an 710129, China
[2]Science and Technology on UAV Laboratory, Northwestern Polytechnical University, Xi'an 710129, China
[3]China Academy of Space Technology (CAST), Beijing 100094, China

Corresponding author: Liangliang Zhao (zll18@mail.nwpu.edu.cn)

This work was supported by the National Natural Science Foundation of China under Grant 62271407.

ABSTRACT In this work, a tapered fed circular-shaped monopole antenna for ultrawideband (UWB) applications integrated with four frequently-used band-notched properties is designed. By the design of notch structures inside the radiation patch, on the feedline, and on either side of the feedline, four notch bands covering from3.3–3.8 GHz, 5.25–5.75 GHz, 7.25–7.75 GHz, and 8.01–8.5 GHz are obtained possibly, which suppress the interference with WiMax, WLAN, satellite downlink and ITU applications, respectively. Based on these, the proposed antenna is operable from 1.4 GHz to 25 GHz with maximum coupling value of -20 dB covering almost operational band, and it has compact dimensions of $43\times36\times1.59$ mm^3. Evolution and accomplishment of final results, involving the reduction of mutual coupling suppression, are illustrated gradually. The property of the monopole antenna considering reflection coefficient, isolation among different ports, realized gain, radiation pattern, efficiency, and envelope correlation coefficient (ECC) are studied. Moreover, experimental results are verified with the simulations. In addition, using the antenna inserted in chest badge, the chance of infection will greatly reduce. Ultimate, the proposed MIMO monopole antenna has a potential application in the medical, high precision machining, and biopharming relevant domains.

INDEX TERMS Band-notched, monopole antenna, MIMO, UWB.

I. INTRODUCTION

With the rapid growing of electronic information system, the demand of wireless communication domain is evolutionary. UWB innovation attracts significant demand due to its wider bandwidth, high information rate, and minimal expense [1]. However, UWB antenna is sensitive to interference signals. Consequently, the antenna with notch band is proposed as the conditions requirement like Worldwide Interoperability for Microwave Access (WiMAX), wireless local area network (WLAN), and X-bands for satellite communication, and so on. The function of band notching is to reject the interference signal in a relatively narrow band [2]. There are plenty of techniques for generating notch bands with various demands. In general, one is to employ parasitic elements, and can introduce current at a prescribed frequency [3], [4], [5], which binds the transmission of Electromagnetic wave and prevents it from radiating, creates a notch band. Additionally, the other is to introducing etch slots into the radiating area, the feed line, and the ground [6], [7], [8], [9], which often promotes current to concentrate near slots and suppress the undesired signals. Unfortunately, the mostly of recent UWB antennas merely generate one [10], [11], two [12], [13] or three notch bands [14], [15], which seems that the amount of notch bands is small. Therefore, by introducing more notch bands, the reliability of the communication system can be sustained

The associate editor coordinating the review of this manuscript and approving it for publication was Jagadheswaran Rajendran.

well, thereby reducing the effect of more interference signals. Meanwhile, the power restriction issues can be addressed by enhancing the channel capacity, and the similar is realizable by Multiple Input-Multiple Output (MIMO) technology. Numerous measures are basically integrated in MIMO antennas to enhance isolation for decreasing the effect of antenna elements. For instance, the diversity technique [16], [17], parasitic components [18], [19], defected ground structure [20], [21], electromagnetic bandgap structure [22], [23], neutralization line [24], [25], and decoupling structures (DS) [26], [27] are the effective methods to improve the isolation. In a word, more notch bands require more complex structures, which can cause disturbance from the various notch structures. For suppressing the interference signals among the different notch structures, choosing the appropriate notch structures is vital for matching every notch band. Although the above works offer numerous antennas with notched band, the operational bandwidth, number of notched band and other relevant properties still need to be improved.

Considering the above issues, the proposed monopole antenna integrated with four frequently-used notch bands is achieved to prevent the corresponding undesired interference signals. Firstly, a tapered fed circular-shaped monopole antenna with etched ground achieves the ultra-wide operating band from 1.4 to 25 GHz. Then, a rectangle shaped slot etched into the circle radiation patch introduces the WiMax band. Two different split-ring resonators (SRRs) located on each side of feedline can applicate in WLAN and satellite downlink band. Furthermore, U-shaped slot etched in feedline can achieve ITU notch band. Moreover, the antenna can be utilized to the less exposure filed such as hospital, high precision machining factory, biological research institution. The rest of this paper is organized as follows. The antenna design and operating principle are depicted in Section II. Section III presents simulation and measurement results, which further validates the correctness of the configuration. Then, the numerous application scenarios of the proposed antenna are illustrated. Finally, Section IV concludes this work.

II. ANTENNA DESIGN AND PARAMETRIC STUDY

The design with a size of L1 × W1. Dielectric constant is 2.2 with a substrate thickness of 1.59 mm. The development of the proposed dual-port monopole MIMO antenna is illustrated through five processes, i.e., Antenna A0 to A4. In the first section, the evolution of the reference antenna (UWB MIMO antenna), is plotted, then generation of first, second, third, fourth notch bands are illustrated step by step, then final antenna configuration is concluded in the last section.

For miniaturizing the monopole antenna, obtaining wideband performance and attaining the four frequently-used band-notched properties, the optimized dimension of the proposed MIMO antenna is listed in Fig. 1 and Table 1.

A. UWB MONOPOLE ANTENNA

In general, the primary design of the antenna originates from choosing the antenna structure. Meanwhile, their sizes of

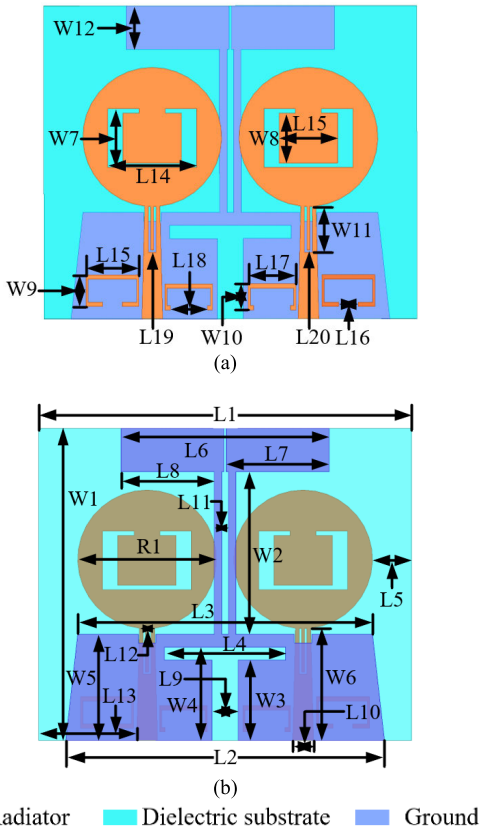

FIGURE 1. Geometry of the proposed MIMO antenna. (a) Front view. (b) Back view.

TABLE 1. Values of optimized parameters of the final antenna.

Parameter	L1	L2	L3	L4	L5	L6	L7	L8
Value(mm)	43	36.76	34	14	15.34	24	11.88	10.75
Parameter	L9	L10	L11	L12	L13	L14	L15	L16
Value(mm)	3	2.4	1.63	1.75	11.3	10.25	6.75	2.25
Parameter	L17	L18	L19	L20	W1	W2	W3	W4
Value(mm)	5.5	4.25	0.9	0.35	36	18.75	9.25	10.75
Parameter	W5	W6	W7	W8	W9	W10	W11	W12
Value(mm)	12.25	12.95	6.75	5.75	3.65	3	5.26	5

the antenna also meet the operational frequency demands properly. Meanwhile, the essential requirement for the UWB antenna is to attain lower cutoff frequency. The approximated equation for computing the fundamental lower resonating frequency of a miniaturized monopole antenna is presented below [28],

$$f_{rL} = \frac{14.4}{L_g + L_p + G + \frac{W_g}{2\pi\sqrt{\varepsilon_r+1}} + \frac{W_p}{2\pi\sqrt{\varepsilon_r+1}}} \quad (1)$$

where f_{rL} represents the lower resonance frequency (GHz), L_g and L_p are the ground length and patch length respectively, G denotes the gap between the radiation patch and ground plane, W_p and W_g denote the area of the radiation patch and ground plane separately. Combined with the data shown in Table 1, the computational frequency f_{rL} is 1.3 GHz, which agrees well with the simulated result as shown in Fig. 2. The evolution of the basic antenna (UWB MIMO) called as A1 is illustrated in Fig. 3. The S11 and S12 of the basic antenna are

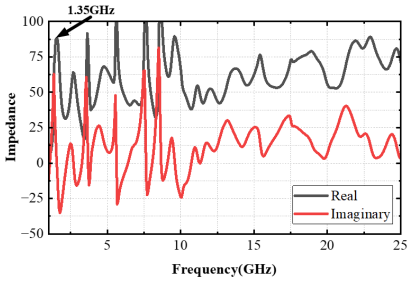

FIGURE 2. Simulated input impedance of the proposed MIMO antenna.

presented in Fig. 4, and Fig. 5, respectively. By employing a T-shaped structure and optimizing the ground area, it can be seen that some resonances appear at around 2 GHz, 14 GHz, 24 GHz in Fig. 3(a). However, the isolation at low-frequency is still deteriorative in Fig. 3(b). Furthermore, in antenna (c), a rectangle slot embedded in T-shaped structure improves the mutual coupling further. After achieving so, the desired lower frequency is realized. Therefore, the antenna(c) is operable from 1.4 GHz to 25 GHz, which across the whole UWB band, with the value of mutual coupling less than −15 dB, and this antenna will be employed as a basic UWB antenna for the generation of notch band in monopole antenna. Meanwhile, as a significant decoupling structure, the effectiveness of ground plane is illustrated in Fig. 6. In Fig. 6(a), it is observed that the coupling currents concentrate more on the entire ground plane for port 1 and port 2. Upon miniaturizing the ground plane space and adding the T-shaped structure, the surface currents with new change mainly collect on the ground plane for port 1, reduces power drift from port 1 to port 2, which in turn causes isolation deteriorated from Fig. 6(b). Unfortunately, combining with Fig. 5, it can be seen that the ground plane with novel structure improves the isolation ranging majority operational band. However, the isolation at around 2GHz is still deteriorated. Moreover, by etching slots on the T-shaped structure and ground plane, more currents concentrate on the added T-shaped structure and less currents flow to port 2. Combing with Fig. 5, the isolation is less than −15 dB covering the whole bandwidth successfully, showing the superior matching characteristics of final UWB antenna (Antenna. A0).

B. BAND-NOTCHED MONOPOLE ANTENNA

For clearly, the proposed antenna with four notched structures is presented by four steps, i.e,. Antenna. A1 to A4, respectively.

1) FIRST-STOP BAND ANTENNA

Firstly, a circular arc-shaped slot is etched in circle radiation patch. Subsequently, a stopband is attained at around 3.5GHz, which names as WiMax band. Meanwhile, the bandwidth coverage and value of mutual coupling are same as Antenna. A0, which presents great performances. These C-shaped slits on etched radiation patch are responsible for the WiMax band, the slits are equivalent to a half-wavelength resonator, and the

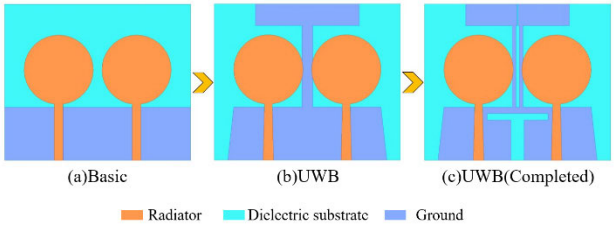

FIGURE 3. The evolution of the reference antenna. (a) Basic antenna. (b) UWB antenna. (c) The optimized UWB antenna (Antenna. A0).

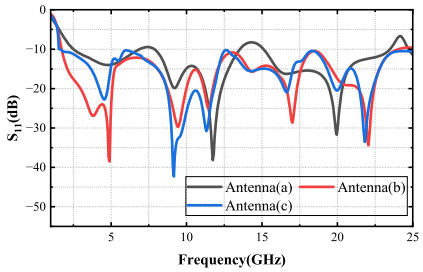

FIGURE 4. The simulated S11 varying with the evolution of the antenna.

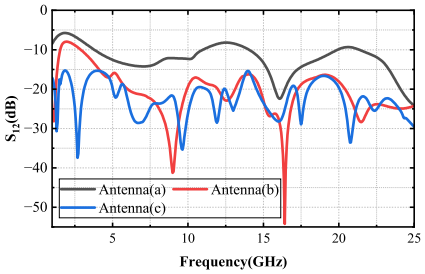

FIGURE 5. The simulated S12 varying with the evolution of the antenna.

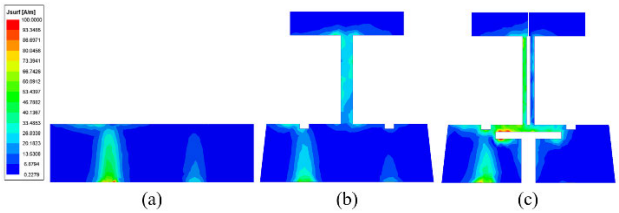

FIGURE 6. Current distributions at 2GHz from various geometries of the ground plane. (a) Basic. (b) UWB. (c) The optimized UWB antenna (Antenna. A0).

length of lower C-shaped slit is computed by:

$$L_{n1} = 2[W7 + L14 + (W7 - W8) + (L14 - L15)] \quad (2)$$

At the same time, the middle of the notched frequencies is approximately by:

$$f_{n1} = \frac{c}{2L_{n1}\sqrt{\varepsilon_r}} \quad (3)$$

2) SECOND-STOP BAND ANTENNA

Furthermore, as shown in Figs. 10, 11, 12, the second notched band is obtained at around 5.5GHz ranging from 5.25 GHz to

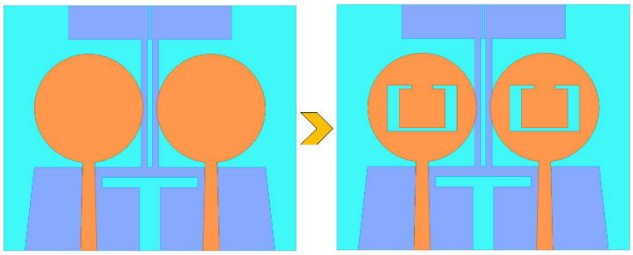

FIGURE 7. The evolution of the single-band notched antenna (Antenna A1).

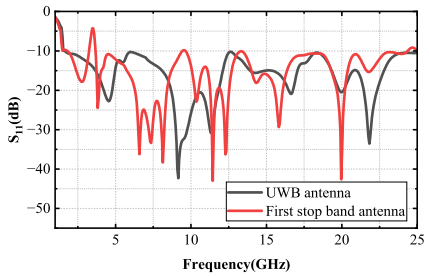

FIGURE 8. The simulated S11 varying with the evolution of the antenna.

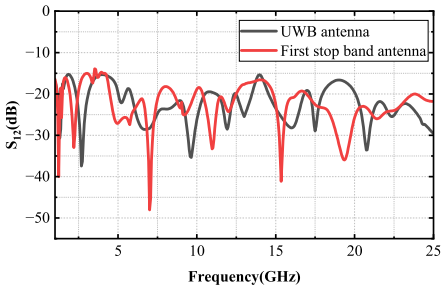

FIGURE 9. The simulated S12 varying with the evolution of the antenna.

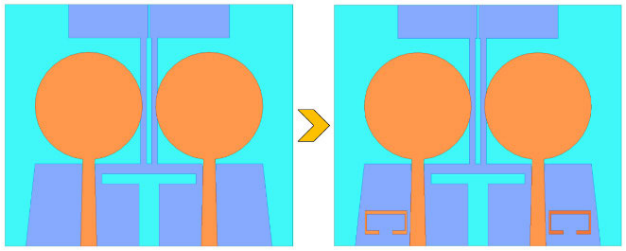

FIGURE 10. The evolution of the second-band notched antenna (Antenna A2).

5.75 GHz by introducing the U-shaped slot on the outside of feedline. Although the second notch band depends on the length and position of U-shaped slot, the level is optimized to sustain S11 below −10 dB across the entire band. Accordingly, the isolation still keeps a low level. Meanwhile, the notched bands exhibit a deteriorated independence value, and the center frequency (CF) of the band-notched can be controlled by different lengths of SRRs. Moreover, the SRRs can be regarded as a quarter-wavelength resonator, where Ln2

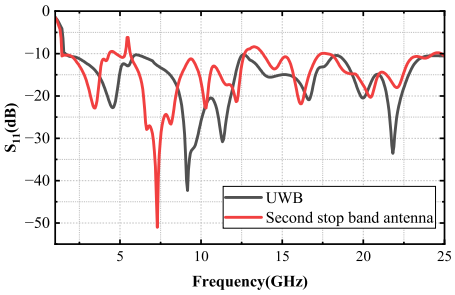

FIGURE 11. The simulated S11 varying with the evolution of the antenna.

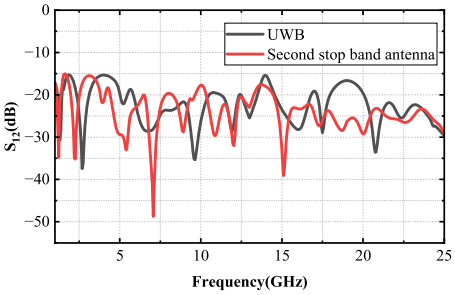

FIGURE 12. The simulated S12 varying with the evolution of the antenna.

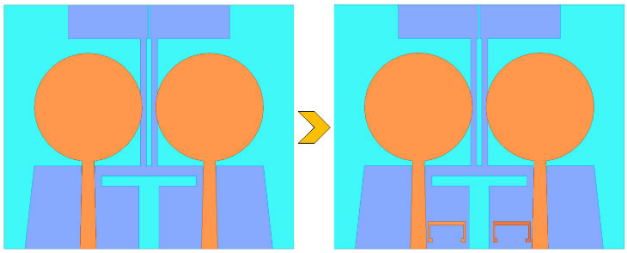

FIGURE 13. The evolution of the third-band notched antenna (Antenna A3)

denotes the length of SRRs and c represent the light speed. In total, the calculated result can be verified by Fig. 11 and Fig. 12.

$$L_{n2} = 2[W9 + L15 + (L15 - L16) + d] \tag{4}$$

$$f_{n2} = \frac{c}{2L_{n2}\sqrt{(\varepsilon_r + 1)/2}} \tag{5}$$

3) THIRD-STOP BAND ANTENNA

Similar, like antenna. A2, other sets of U-shaped slots on the inside of the feedline employed obtain a notch band at around 7.5 GHz, which names as satellite downlink band. Due to the small distance to feedline, there is negligible effect on the upper impedance band, which deteriorates the operating band at around 23 GHz. In the meantime, the length of SRRs also can be calculated by following equations, and the optimized result can be shown in Figs. 14 and 15.

$$L_{n3} = 2[W10 + L17 + (L17 - L18) + d] \tag{6}$$

$$f_{n3} = \frac{c}{2L_{n3}\sqrt{(\varepsilon_r + 1)/2}} \tag{7}$$

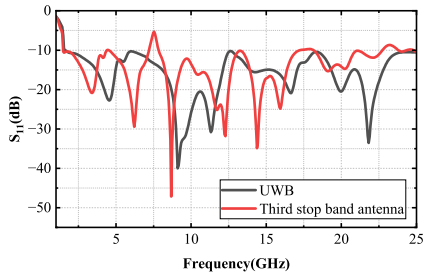

FIGURE 14. The simulated S11 varying with the evolution of the antenna.

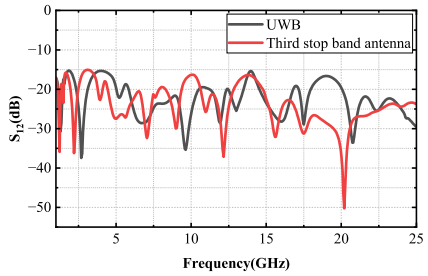

FIGURE 15. The simulated S12 varying with the evolution of the antenna.

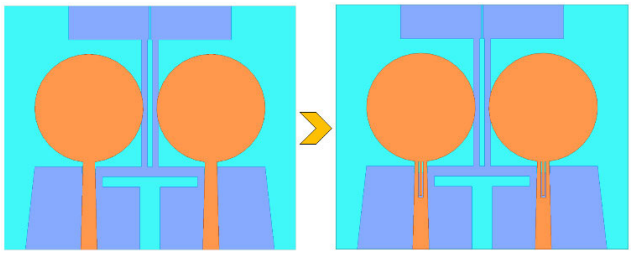

FIGURE 16. The evolution of the fourth-band notched antenna (Antenna A4).

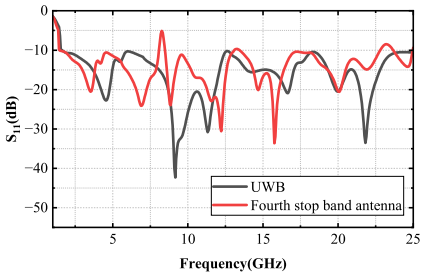

FIGURE 17. The simulated S11 varying with the evolution of the antenna.

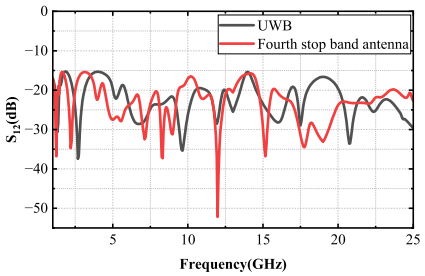

FIGURE 18. The simulated S12 varying with the evolution of the antenna.

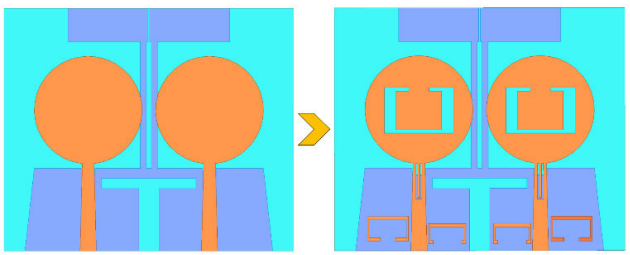

FIGURE 19. Dimension of the proposed antenna (Antenna A5).

4) FOURTH-STOP BAND ANTENNA

Besides, a small U-shaped slot etched in the feedline offers the ITU notched band. There is a slightly effect of this slot on reflection coefficient. Therefore, the notched monopole antenna attaining an impedance bandwidth covers from 1.4 GHz to 23 GHz. In addition, the U-shaped slot can be calculated as follows

$$L_{n4} = 2[W11 + L20 + d1 + d1] \tag{8}$$

$$f_{n4} = \frac{c}{2L_{n4}\sqrt{\varepsilon_r}} \tag{9}$$

Furthermore, by optimizing the slot etched on the feedline, the fourth stop band can be plotted in Fig. 17 and Fig. 18.

5) FINAL PROPOSED DESIGN

Based on the Antenna A0, Antenna A1, Antenna A2, Antenna A3, and Antenna A4 are combined to form the final proposed antenna. The S-parameters are illustrated in Fig. 20 and Fig. 21, and the optimized parameter values are presented in Table 1. Small differences existing in the final antenna performances is tolerable. By designing and optimizing the MIMO antenna appropriately, the final antenna realizes an ultra-wideband from 1.4 GHz to 25 GHz with four stop bands at 3.5 GHz (3.3–3.7 GHz), 5.5 GHz (5.2–5.8 GHz), 7.5 GHz (7.25-7.75 GHz) and 8.25GHz (8.01-8.5 GHz). The results are optimized due to the effects of different notch band structures, but the influence is negligible. Consequently, by the comparison with results of the UWB-MIMO Antenna A0 (Reference Antenna), which facilitate the expiations of notched bands in detail. The mutual coupling is more diminutive than −20 dB for the entire band except for low-frequency band, more diminutive than −15 dB.

From Antenna A1 to A4, the number of notched bands gradually enhances, and the notch band moves to the high band. These intending that the notching property of the monopole antenna is slowly distinct.

Antenna. A5 as the final edition of the proposed UWB MIMO antenna integrated with four commonly notched band. The size of monopole antenna is 43 mm∗36 mm∗1.59 mm. HFSS 2021 is utilized to simulate and verify the proposed antenna. Fig. 22 presents the surface current distributions at four notch frequency points, where (a), (b), (c) and (d) show the current distribution of proposed antenna at 3.5, 5.5,

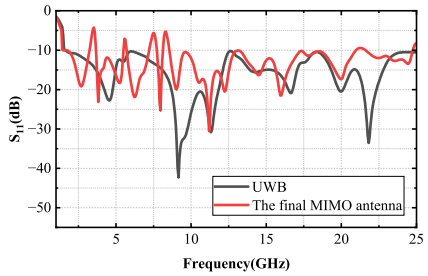

FIGURE 20. The simulated S11 varying with the evolution of the antenna.

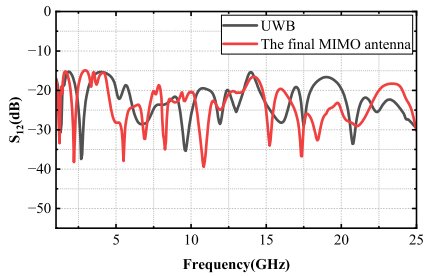

FIGURE 21. The simulated S12 varying with the evolution of the antenna.

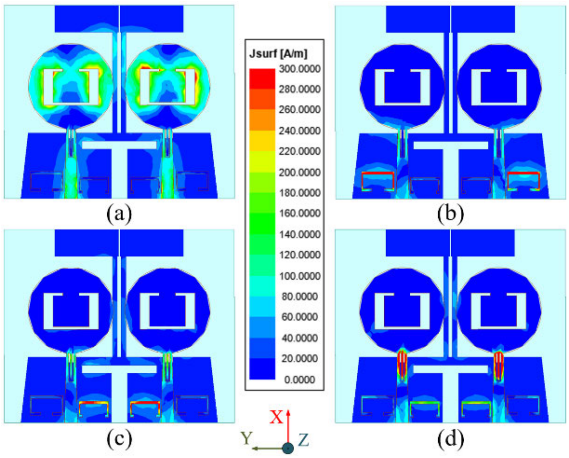

FIGURE 22. Magnitude surface current distributions at (a) 3.5, (b) 5.5, (c) 7.5, and (d) 8.3 GHz.

7.5, 8.3 GHz, respectively. The current is mostly distributed on the rectangle strip in the radiating patch at 3.5 GHz. Then, at 5.5 GHz, the current is mostly distributed on the U-shaped slot outside of feed line. Similar, the surface current is mainly distributed on the U-shaped slot inside of feed line at 7.5 GHz. Furthermore, the current is mainly scattered on a small U-shaped slot etched in the feedline at 8.3 GHz. The above structures effectively boost realizing the four notch bands UWB MIMO monopole antenna.

III. RESULTS AND DISCUSSION

Fig. 23 presents the prototype and measurement of the antenna, Fig. 24 provides the simulation and experimental results of S-parameters of the proposed antenna, which plots

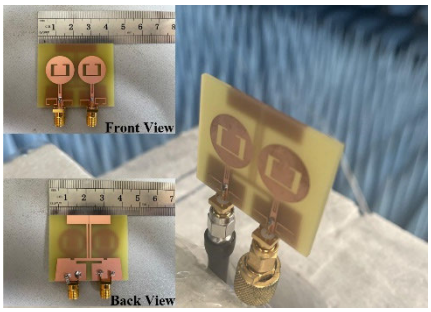

FIGURE 23. Fabricated antenna and its measurement view.

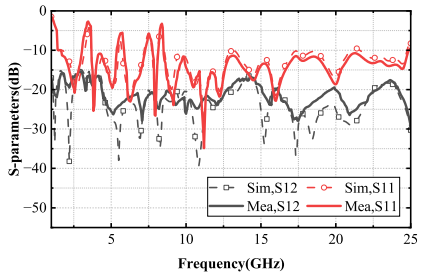

FIGURE 24. The simulated and measured S-parameters.

the magnitude of the reflction coeffcient (|S11|) of the four notch bands UWB antenna.

The bandwidth of S11< −10 across from 1.4 to 25 GHz. Meanwhile, the measured mutual coupling is less than -15dB ranging the operational band. The notch bands of the antenna cover 3.3−3.8 GHz, 5.25−5.75 GHz, 7.25−7.75 GHz, and 8.01−8.5 GHz, respectively. The four notch bands reject the interference signals with effect, such as WiMax (3.3−3.8 GHz), WLAN (5.25–5.75 GHz), satellite downlink (7.25-7.75 GHz) and ITU (8.01-8.5 GHz) applications. The whole results demonstrate that the antenna has superior band-notched properties and high isolation performance. However, the fluctuating S-parameters of the antenna at some frequencies between measurements and simulations are resulted from the errors of experiment and fabricating.

As seen in Fig. 25, the radiation patterns of proposed antenna at 3 GHz, 4.5 GHz and 6 GHz are presented. It is observed that the pattern is quasi-omnidirectional in XOY and YOZ planes. Moreover, the pattern is bidirectional in XOZ plane. At the same time, the measured cross polarization at the main beam direction is all below −20 dB. Besides, the simulated and measured results fit well, indicating the antenna has great radiation performances.

When the first port is excited and the second port is terminated, the simulated and measured antenna gain and radiation effciency are illustrated in Fig. 26 and Fig. 27, respectively. In all four notch frequency bands, the values of realized gain are negative, which intensely shows that the antenna has superior notch property. Then, in other operational frequency bands, the value of gain surpasses 0, showing that the antenna has distinguished radiation performances. The peak gain of

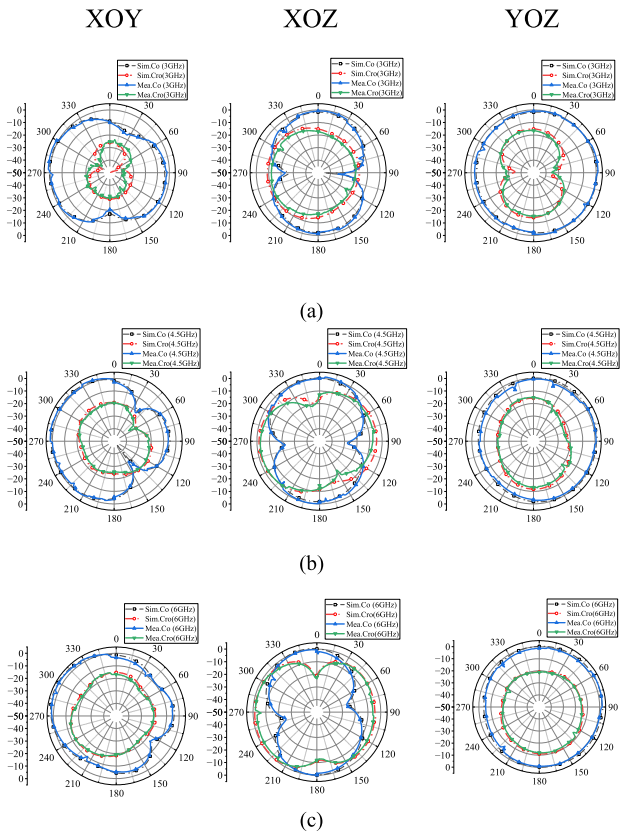

FIGURE 25. Simulated and measured radiation patterns of XOY, XOZ, YOZ planes. (a) 3GHz. (b) 4.5GHz. (c) 6GHz.

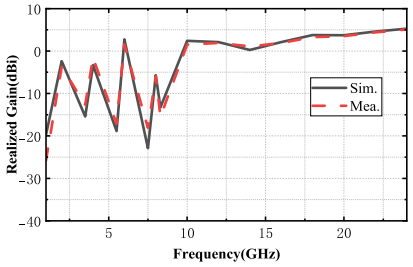

FIGURE 26. Simulated and measured realized gain.

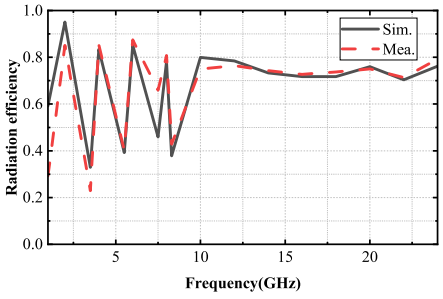

FIGURE 27. Simulated and measured radiation efficiency.

the antenna achieves 5.1 dBi. For the entire band, radiation efficiency is greater than 75%, excluding the notch bands. The human model has slight interference on the transmission

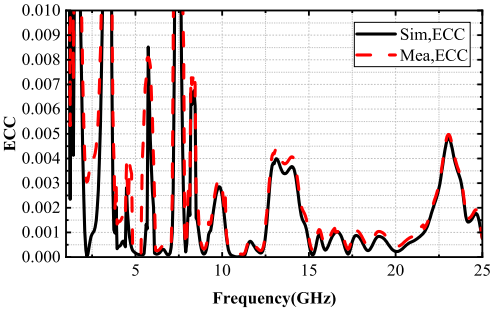

FIGURE 28. Simulated and measured ECC varies with frequency.

TABLE 2. Performance comparison of different antennas.

Ref.	Dimension	BW. (GHz)	No. of notch bands	ECC	Gain (dBi)	Efficiency
[29]	0.214 λ_{low}×0.256 λ_{low} ×0.004 λ_{low} (30mm× 25mm×0.508mm)	2.56-12.7	5	NG	4.76	>75%
[30]	0.383 λ_{low}×0.383 λ_{low} ×0.009 λ_{low} (35.9mm ×35.9mm×0.8mm)	3.2-10.8	3	<0.49	4.7	>80%
[31]	0.788 λ_{low}×1.035 λ_{low} ×0.035 λ_{low} (35mm × 46mm × 1.575mm)	2.1-11.4	2	<0.04	NG	>75%
[32]	0.25 λ_{low} ×0.25 λ_{low}×0.006 λ_{low} (30mm× 30mm×0.7mm)	2.5-10.8	2	<0.004	4.9	>80%
[33]	0.245 λ_{low} ×0.192 λ_{low}×0.008 λ_{low} (46mm*36mm*1.59mm)	1.6-16	2	<0.1	NG	NG
This work	0.2 λ_{low}×0.168 λ_{low}× 0.007 λ_{low} (43mm× 36mm×1.59mm)	1.4-25	4	<0.005	5.1	>75%

of Electromagnetic waves. Nevertheless, the problems are within the presentable region. It is can be seen that minimum efficiency and minimum gain are realized at the stopbands. The antenna has an extraordinary omnidirectional characteristic with no obvious distortions at high band. Although there are several differentials, it is observed that the experimented results and simulated results are basically similar. Meanwhile, combined with measured S-parameters and then calculated by equation (10), the ECC value of the proposed antenna below 0.004 exclude the notched bands in Fig. 28, intending that the antenna has superior signal independence.

$$ECC = \frac{\left|S_{11}^{*}S_{12} + S_{21}^{*}S_{22}\right|^{2}}{(1-|S_{11}|^{2}-|S_{21}|^{2})(1-|S_{22}|^{2}-|S_{12}|^{2})} \quad (10)$$

Antenna A5 is compared with practical monopole antennas in the work, and the comparison is listed in Table 2. It is can be seen that the proposed antenna has the largest operational wideband, the most compact dimension. Moreover, it also has more frequently-used notched bands and the lower ECC, providing stable radiation characteristics. In a word, the novel structure shows the final antenna as a superior applicant for UWB domains with MIMO properties.

IV. ANTENNA APPLICATION SCENARIO

As shown in Fig. 29, in some specific scenarios such as hospital, integrated-circuit (IC) manufacturing factory,

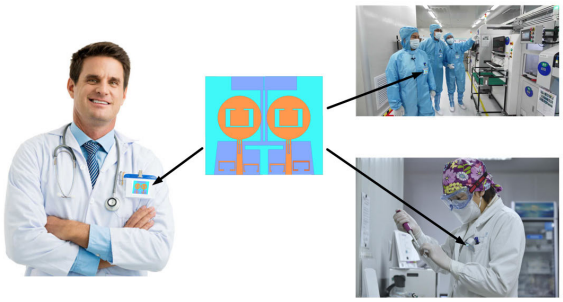

FIGURE 29. Application of the proposed antenna.

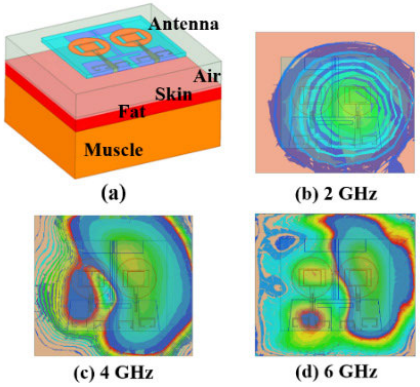

FIGURE 30. Illustration of the proposed antenna over the (a) human tissue in HFSS and SAR distributions at (b) 2GHz, (c) 4GHz, (d) 6 GHz.

and biopharmaceutical company, the environments of these places are expected to avoid bacterial and dust pollution. However, the chest badge is often taken off, picked up, or brought out to replace a new one. Meanwhile, these behaviors can enhance the risk of cross infection. Therefore, the proposed antenna provides a practical solution toward the realization of reducing replacement of chest badge and decreasing the risk of bacterial infection.

In addition, the SAR level of the proposed antenna deserves attention, and it determines whether the monopole antenna has resulted in radiation insult to people health, due to the short distance between chest badge and body. Then the SAR level experimental is illustrated in Fig. 30(a). In common, the simulated people body model is comprised of three layers, called skin, fat, and muscle. Meanwhile, three tissues have the thicknesses of 1, 5, and 20 mm separately, a sum of 26 mm body. Between the model and the antenna, the air layer with the thickness of 10 mm is similar to a certain gap from body to clothes. According to the US IEEE C.95-1999 standard, the value of SAR should be maintained below 1.6 W/kg per 1g tissue, which is stricter than EUR standard. The result of SAR level at 2, 4, 6 GHz is simulated in Fig. 30.

As shown in Table 3, the proposed antenna has a safe performance and wearing it on the chest is suitable for body, which is potential for multi-scenario application, i.e,. medical development, high precision manufacturing in dust-free environment, biomedical field and so on.

TABLE 3. Maximum sar and maximum input power.

Frequency (GHz)	1g Tissue [W/kg]/Input power [W]
2	1.45/0.08
4	1.52/0.12
6	1.49/0.22

V. CONCLUSION

A compact dual-port UWB MIMO circular-shaped monopole antenna with four frequently-used notch bands is introduced and analyzed. Firstly, proposed antenna realizes a ultrawide operational band from 1.4-25 GHz. Then, employing notch structures inside the radiation patch, feedline, and either side of feedline, a four notch bands antenna is achieved. Meanwhile, detailed construction and achievement of results are discussed. Furthermore, the proposed antenna has overall size of 0.2 $\lambda_{low}\times 0.168\ \lambda_{low}\times 0.007\ \lambda_{low}$ (43 mm$\times$36 mm$\times$1.59 mm), which is compact. The measured results present that the proposed antenna can range the entire UWB spectrum except notch bands from 3.3 to 3.8 GHz (WiMax), 5.25 to 5.75 GHz (WLAN), 7.25 to 7.75 GHz (satellite downlink), and 8.01 to 8.5 GHz (ITU). The ECC is less than 0.004, whereas measured mutual coupling is less than -20 dB in its majority operation bandwidth. In total, the above results suggest that the great potential of the antenna can be extensively utilized in UWB-MIMO communication domain for portable application scenarios. Besides, the proposed antenna can be employed in medical, high precision machining, and biopharming relevant domains.

REFERENCES

[1] I. B. Vendik, A. Rusakov, K. Kanjanasit, J. Hong, and D. Filonov, "Ultrawideband (UWB) planar antenna with single-, dual-, and triple-band notched characteristic based on electric ring resonator," *IEEE Antennas Wireless Propag. Lett.*, vol. 16, pp. 1597–1600, 2017.

[2] L. Kang, H. Li, X. Wang, and X. Shi, "Compact offset microstrip-fed MIMO antenna for band-notched UWB applications," *IEEE Antennas Wireless Propag. Lett.*, vol. 14, pp. 1754–1757, 2015.

[3] O. P. Kumar, P. Kumar, and T. Ali, "A compact dual-band notched UWB antenna for wireless applications," *Micromachines*, vol. 13, no. 1, p. 12, Dec. 2021.

[4] L. Cui, H. Liu, C. Hao, and X. Sun, "A novel UWB antenna with triple band-notches for WiMAX and WLAN," *Prog. Electromagn. Res. Lett.*, vol. 82, pp. 101–106, 2019.

[5] V. N. K. R. Devana and A. M. Rao, "A novel fan shaped UWB antenna with band notch for WLAN using a simple parasitic slit," *Int. J. Electron. Lett.*, vol. 7, no. 3, pp. 352–366, Jul. 2019.

[6] W. A. Awan, A. Zaidi, N. Hussain, A. Iqbal, and A. Baghdad, "Stub loaded, low profile UWB antenna with independently controllable notch-bands," *Microw. Opt. Technol. Lett.*, vol. 61, no. 11, pp. 2447–2454, Nov. 2019.

[7] A. Iqbal, A. Smida, N. Mallat, M. Islam, and S. Kim, "A compact UWB antenna with independently controllable notch bands," *Sensors*, vol. 19, no. 6, p. 1411, Mar. 2019.

[8] G. Kumar, D. Singh, and R. Kumar, "A planar CPW fed UWB antenna with dual rectangular notch band characteristics incorporating U-slot, SRRs, and EBGs," *Int. J. RF Microw. Comput.-Aided Eng.*, vol. 31, no. 7, Jul. 2021, Art. no. e22676.

[9] S. Raziul Ahasan, K. Islam, M. Monirujjaman Khan, M. Masud, G. Singh Gaba, and H. A. Alhumyani, "Novel compact UWB band notch antenna design for body-centric communications," *Comput. Syst. Sci. Eng.*, vol. 40, no. 2, pp. 673–689, 2022.

[10] H. Qi and H. Liu, "Single-ended band-notched Vivaldi antenna with common mode suppression and low cross polarization," *IEEE Antennas Wireless Propag. Lett.*, vol. 20, no. 10, pp. 1983–1987, Oct. 2021.
[11] Y. Xu, J. Wang, L. Ge, X. Wang, and W. Wu, "Design of a notched-band Vivaldi antenna with high selectivity," *IEEE Antennas Wireless Propag. Lett.*, vol. 17, pp. 62–65, 2018.
[12] Z. A. A. Hassain, M. M. Ali, and A. R. Azeez, "Single and dual band-notch UWB antenna using SRR /CSRR resonators," *J. Commun.*, vol. 14, no. 6, pp. 504–510, Jun. 2019.
[13] A. Ghosh, G. Sen, M. Kumar, and S. Das, "Design of UWB antenna integrated with dual GSM functionalities and dual notches in the UWB region using single branched EBG inspired structure," *IET Microw., Antennas Propag.*, vol. 13, no. 10, pp. 1564–1571, Aug. 2019.
[14] A. Ghosh, T. Mandal, and S. Das, "Design and analysis of triple notch ultrawideband antenna using single slotted electromagnetic bandgap inspired structure," *J. Electromagn. Waves Appl.*, vol. 33, no. 11, pp. 1391–1405, Apr. 2019.
[15] S. Lakrit, S. Das, S. Ghosh, and B. T. P. Madhav, "Compact UWB flexible elliptical CPW-fed antenna with triple notch bands for wireless communications," *Int. J. RF Microw. Comput.-Aided Eng.*, vol. 30, no. 7, Jul. 2020, Art. no. e22201.
[16] L. Liu, S. W. Cheung, and T. I. Yuk, "Compact MIMO antenna for portable UWB applications with band-notched characteristic," *IEEE Trans. Antennas Propag.*, vol. 63, no. 5, pp. 1917–1924, May 2015.
[17] Y. Sharma, D. Sarkar, K. Saurav, and K. V. Srivastava, "Three-element MIMO antenna system with pattern and polarization diversity for WLAN applications," *IEEE Antennas Wireless Propag. Lett.*, vol. 16, pp. 1163–1166, 2017.
[18] A. Iqbal, O. A. Saraereh, A. W. Ahmad, and S. Bashir, "Mutual coupling reduction using F-shaped stubs in UWB-MIMO antenna," *IEEE Access*, vol. 6, pp. 2755–2759, 2018.
[19] M. S. Khan, A.-D. Capobianco, S. M. Asif, D. E. Anagnostou, R. M. Shubair, and B. D. Braaten, "A compact CSRR-enabled UWB diversity antenna," *IEEE Antennas Wireless Propag. Lett.*, vol. 16, pp. 808–812, 2017.
[20] J.-F. Li, Q.-X. Chu, and T.-G. Huang, "A compact wideband MIMO antenna with two novel bent slits," *IEEE Trans. Antennas Propag.*, vol. 60, no. 2, pp. 482–489, Feb. 2012.
[21] V. Satam and S. Nema, "Two element compact UWB diversity antenna with combination of DGS and parasitic elements," *Wireless Pers. Commun.*, vol. 98, no. 3, pp. 2901–2911, Feb. 2018.
[22] S. Ghosh, T.-N. Tran, and T. Le-Ngoc, "Dual-layer EBG-based miniaturized multi-element antenna for MIMO systems," *IEEE Trans. Antennas Propag.*, vol. 62, no. 8, pp. 3985–3997, Aug. 2014.
[23] S. R. Thummaluru, R. Kumar, and R. K. Chaudhary, "Isolation enhancement and radar cross section reduction of MIMO antenna with frequency selective surface," *IEEE Trans. Antennas Propag.*, vol. 66, no. 3, pp. 1595–1600, Mar. 2018.
[24] S. Zhang and G. F. Pedersen, "Mutual coupling reduction for UWB MIMO antennas with a wideband neutralization line," *IEEE Antennas Wireless Propag. Lett.*, vol. 15, pp. 166–169, 2016.
[25] W. Huey Shin, S. Kibria, and M. Tariqul Islam, "Hexa band MIMO antenna with neutralization line for LTE mobile device application," *Microw. Opt. Technol. Lett.*, vol. 58, no. 5, pp. 1198–1204, May 2016.
[26] B. C. Pan and T. J. Cui, "Broadband decoupling network for dual-band microstrip patch antennas," *IEEE Trans. Antennas Propag.*, vol. 65, no. 10, pp. 5595–5598, Oct. 2017.
[27] J. Baek and J. Choi, "The design of a LTE/MIMO antenna with high isolation using a decoupling network," *Microw. Opt. Technol. Lett.*, vol. 56, no. 9, pp. 2187–2191, Sep. 2014.
[28] J.-F. Li, Q.-X. Chu, Z.-H. Li, and X.-X. Xia, "Compact dual band-notched UWB MIMO antenna with high isolation," *IEEE Trans. Antennas Propag.*, vol. 61, no. 9, pp. 4759–4766, Sep. 2013.
[29] Z. Zhao, C. Zhang, Z. Lu, H. Chu, S. Chen, M. Liu, and G. Li, "A miniaturized wearable antenna with five band-notched characteristics for medical applications," *IEEE Antennas Wireless Propag. Lett.*, vol. 22, no. 6, pp. 1246–1250, Jun. 2023.
[30] S. Jayant and G. Srivastava, "Close-packed quad-element triple-band-notched UWB MIMO antenna with upgrading capability," *IEEE Trans. Antennas Propag.*, vol. 71, no. 1, pp. 353–360, Jan. 2023.
[31] M. Agarwal, J. K. Dhanoa, and M. K. Khandelwal, "Two-port hexagon shaped MIMO microstrip antenna for UWB applications integrated with double stop bands for WiMax and WLAN," *AEU-Int. J. Electron. Commun.*, vol. 138, Aug. 2021, Art. no. 153885.
[32] H. Yuan, F. S. Zhang, J. J. Zhang, Y. X. Feng, and Y. F. Liu, "A compact ultra-wideband multiple-input-multiple-output antenna with dual band-notched performance using slot-line transmission," *Int. J. RF Microw. Comput.-Aided Eng.*, vol. 32, no. 5, 2022, Art. no. e23098.
[33] A. Kholapure and R. G. Karandikar, "Printed MIMO antenna with reconfigurable single and dual band notched characteristics for cognitive radio," in *Proc. IEEE Int. Conf. Antenna Innov. Modern Technol. Ground, Aircraft Satellite Appl.*, Nov. 2017, pp. 1–5.
[34] L. Zhao, H. Zhu, H. Zhao, G. Liu, K. Wang, J. Mou, W. Zhang, and J. Li, "Design of wideband dual-polarized ME dipole antenna with parasitic elements and improved feed structure," *IEEE Antennas Wireless Propag. Lett.*, vol. 22, pp. 174–178, 2023.
[35] M. Yang, H. Peng, K. Zheng, and G. Wei, "Spatial radiation field distribution of underwater VLF two-element antenna array," *IEEE Trans. Antennas Propag.*, vol. 71, no. 1, pp. 1164–1169, Jan. 2023.
[36] L. L. Zhao, C. Hu, C. Fang, C. Fan, J. Li, and A. Li, "Grid restoration algorithm to improve PO calculation accuracy in GRECO," in *Proc. Cross Strait Radio Sci. Wireless Technol. Conf. (CSRSWTC)*, Fuzhou, China, 2020, pp. 1–3.
[37] J. Li, L. Zhao, X. Liu, and Y. Li, "FSV-based evaluation of electromagnetic scattering characteristics of deformed target," in *Proc. Int. Appl. Comput. Electromagn. Soc. Symp.*, Nanjing, China, 2019, pp. 1–2.
[38] L. Zhao, C. Liu, C. Li, D. Song, Y. Wang, Y. Liang, H. Zhao, and C. Hu, "A novel helical antenna for high-power design in X-band," *AEU-Int. J. Electron. Commun.*, vol. 168, Aug. 2023, Art. no. 154725.

LIANGLIANG ZHAO received the M.S. degree in electromagnetic fields and microwave technology from Northwestern Polytechnical University, Xi'an, China, in 2021, where he is currently pursuing the Ph.D. degree in electronic science and technology.

His current research interests include wideband antenna design, antenna array optimization algorithm development for beamforming, and computational electromagnetic.

YONGMAO WANG was born in Shandong, China, in 1999. He received the B.S. degree in electronic science and technology from Harbin University of Science and Technology, Harbin, China, in 2022. He is currently pursuing the master's degree in electronic information with Northwestern Polytechnical University, Xi'an, China.

His current research interests include broadband antenna design and antenna array.

CHENLU LIU was born in Shaanxi, China, in 1999. She received the B.S. degree in electronic information engineering from China University of Geosciences, Beijing, China, in 2021. She is currently pursuing the master's degree in electromagnetic field and microwave technology with Northwestern Polytechnical University, Xi'an, China.

Her current research interests include antenna design and antenna array algorithms.

DENGYANG SONG was born in Henan, China, in 1999. He received the B.S. degree in electronic science and technology from North China University of Water Resources and Electric Power, Zhengzhou, China, in 2021. He is currently pursuing the master's degree in electronic information with Northwestern Polytechnical University, Xi'an, China.

His current research interests include antenna array synthesis and antenna design.

CHUFENG HU received the B.Sc., M.Sc., and Ph.D. degrees from Northwestern Polytechnical University, in 2004, 2007, and 2010, respectively.

He is currently a Professor with Northwestern Polytechnical University. His research interests include radar cross-section measurement, microwave imaging and radar remote sensing, and antenna design.

CHUWEI LI was born in Shanxi, China, in 1997. She received the B.Sc., M.S., and M.Sc. degrees in electromagnetic fields and microwave technology from Northwestern Polytechnical University, Xi'an, China, in 2019, 2019, and 2022, respectively.

She is currently with China Academy of Space Technology (CAST), Beijing, China. Her research interests include radar cross-section measurement, microwave imaging and radar remote sensing, and antenna design.

HUILING ZHAO was born in Shaanxi, China, in 1967. She received the Ph.D. degree in circuit and systems from Northwestern Polytechnical University, Xi'an, China, in 2002.

From 2006 to 2007, she was a Visiting Associate Professor with Duke University, Durham, NC, USA. She is currently a Professor with the School of Electronics and Information, Northwestern Polytechnical University. Her current research interests include ultrawideband antenna design, optimization algorithm development for beamforming, and computational electromagnetic.

ZEFANG WANG was born in Anhui, China, in 1993. He received the B.S. degree in optoelectronic information science and engineering from Hefei Normal University, Hefei, China, in 2017, and the M.S. degree in optical engineering computer technology from the University of Shanghai for Science and Technology, Shanghai, China, in 2021.

His current research interests include IC design and antenna design.